

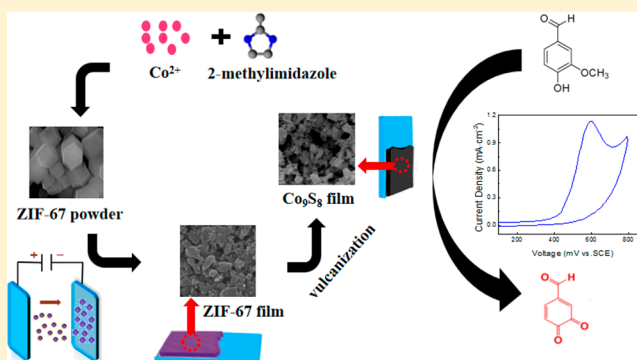
# Preparation of a ZIF-67 Derived Thin Film Electrode via Electrophoretic Deposition for Efficient Electrocatalytic Oxidation of Vanillin

Haijuan Han, Xiaoxuan Yuan, Zhixin Zhang, and Jingbo Zhang\*<sup>ID</sup>

Key Laboratory of Inorganic–Organic Hybrid Functional Material Chemistry, Ministry of Education, Tianjin Key Laboratory of Structure and Performance for Functional Molecules, College of Chemistry, Tianjin Normal University, Tianjin 300387, China

## Supporting Information

**ABSTRACT:** The electrophoretic deposition method is employed to deposit uniform metal organic framework thin films. ZIF-67 particles dispersed in isopropanol move to a cathode as an electric field is applied on two conducting glass electrodes, the uniform ZIF-67 thin film can be formed on the conducting glass substrate. As the deposition time is fixed at 1 min, the prepared film thickness can be adjusted from 1.0 to 7.0  $\mu\text{m}$  by applying different electric fields from 20 to 60  $\text{V}\cdot\text{cm}^{-1}$ . The deposited ZIF-67 thin film is further converted into porous  $\text{Co}_9\text{S}_8$  thin films by the vulcanization with S powder. The porous thin films vulcanized at different temperatures are characterized by the measurements of scanning electron microscope, X-ray photoelectron spectroscopy, X-ray powder diffraction, high resolution transmission electron microscopy, and Fourier transform infrared spectra. The prepared porous  $\text{Co}_9\text{S}_8$  thin films are used as the thin film electrode to catalyze the degradation of vanillin. The  $\text{Co}_9\text{S}_8$  thin film vulcanized at 500  $^\circ\text{C}$  shows better catalytic performance than the bare glassy carbon electrode and the electrodes vulcanized at other temperatures. The electrocatalytic degradation enhancement mechanism is analyzed by the measurements of Tafel curves and electrochemical impedance spectroscopies. It can be developed as a feasible method for the electrocatalytic detection of vanillin.



## 1. INTRODUCTION

Metal organic frameworks (MOFs), as a new type of periodic porous materials formed through self-assembly of metal ions and organic ligands, have been applied in some fields such as gas storage,<sup>1</sup> separation,<sup>2</sup> catalysis,<sup>3</sup> chemical sensing,<sup>4</sup> and proton conduction.<sup>5</sup> In recent years, copper or cobalt-based MOFs were used excellent precursors or sacrificial templates to construct porous functional materials for electrochemical catalysis.<sup>6</sup> As a subfamily of MOFs, zeolitic imidazolate frameworks (ZIFs) created by bridging N-containing imidazolate linkers and zinc or cobalt ions within tetrahedral frameworks have attracted great attention. They have been utilized for selective syntheses of porous carbon, metal oxides, and metal sulfide nanocomposites that have promising applications in catalytic aspects.<sup>7</sup>

For some applications such as chemical sensing,<sup>8</sup> batteries,<sup>9</sup> and supercapacitors,<sup>10</sup> a MOF film is a requirement; therefore, studying the preparation of MOF thin films has become a hot research topic. Fabricating MOF thin films on the desired substrate is a crucial challenge. In addition, the MOF thin films grown on solid substrates have several advantages over the powder samples. As chemical catalysis, they are easily separated from the liquid medium and the number of catalytic active sites at each MOF thin film is approximately constant.<sup>11</sup> Recently, some interesting methods to fabricate MOF thin

films have been explored, such as direct solvothermal,<sup>12</sup> layer by layer or liquid phase epitaxy,<sup>13</sup> electrochemical deposition,<sup>14</sup> microwave-induced thermal deposition, electrospinning,<sup>15</sup> and hot-pressing.<sup>16</sup> Although each method has its advantages, no method has been proved to be universally applicable. Therefore, it is very challenging to find a quick and ease preparation method of MOF thin films on the unmodified low cost substrate.

Electrophoretic deposition (EPD) has attracted wide attention due to its lower cost, short fabrication time, effectively controlled thickness and uniformity of the obtained films, and ease of scaling up. In the EPD process, the charged particles move to the oppositely charged electrode and deposit on the base surface under an applied electric field. It is an economical and universal processing technique that has already been applied to deposit coatings and films such as phosphor for display.<sup>17</sup>

Vanillin (4-hydroxy-3-methoxybenzaldehyde) is derived from the beans or pods of tropical vanilla orchids and used as an indispensable smell additive in a wide range of products such as beverages, milk powders, confectionery, and cosmetics.<sup>18</sup> In addition, vanillin has been used to treat a

Received: November 23, 2018

variety of diseases, including stress, digestive problems, anxiety, stomach pain, and vomiting.<sup>19</sup> Although vanillin is widely used in our lives, too much ingestion of vanillin can have serious adverse effects on our bodies and affect the function of the liver and kidney.<sup>20</sup> Therefore, the simple and low-cost determination of vanillin content is of great significance to people's health. Several methods to detect vanillin have been reported such as ultraviolet–visible spectrum,<sup>21</sup> gas chromatography,<sup>22</sup> and colorimetric<sup>23</sup> and electrochemical techniques.<sup>18</sup> Among these techniques, the electrochemical technique is simple, low cost, and rapid for the determination of vanillin.<sup>19</sup> Some chemically modified glassy carbon electrodes (GCE) have been employed. However, their performance was still not enough good.<sup>24</sup> Thus, it is important to search for a rapid and efficient detection way of vanillin with new materials such as nanomaterials.

Here, we deposited ZIF-67 powders on conducting glass using the EPD method to prepare large-scale, uniform, and continuous thin films and the film thickness can be adjusted by applying different electric fields. Especially, isopropanol is used as a dispersant with the advantages of low pollution and large-scale production compared to the previously reported toluene and dichloromethane dispersants.<sup>25,26</sup> Moreover, the used the EPD process has the advantages of short time and low electric field. For example, it only takes 1 min to complete the film preparation under  $20 \text{ V}\cdot\text{cm}^{-1}$ . The as-prepared films are then used as the sacrificial templates and react with sulfur powders under nitrogen to form porous cobalt sulfide thin film, which could subsequently act as electrode for electrocatalytic oxidation of vanillin. It provided a viable way to detect vanillin through a thin film electrode.

## 2. EXPERIMENTAL SECTION

**2.1. Electrophoretic Deposition of ZIF-67 Thin Films.** All the chemicals were directly used after purchase without further purification. ZIF-67 particles powder was synthesized in an ambient condition according to the reported method.<sup>27</sup> Solution A was prepared by dissolving 2.9 g  $\text{Co}(\text{NO}_3)_2\cdot 6\text{H}_2\text{O}$  in 100 mL methanol. Solution B was formed by dissolving 6.5 g 2-methylimidazole in 100 mL methanol. In a typical synthesis process of ZIF-67, the solution B was added to the solution A under vigorous stirring at room temperature, and the stirring was kept for 1 h. After the resultant mixed solution was aged at room temperature for 24 h, the purple precipitate was collected by the centrifugation, washed three times with fresh methanol, and then dried at  $80 \text{ }^\circ\text{C}$  in vacuum for 12 h.

In order to prepare the ZIF-67 suspension for EPD, 100 mg ZIF-67 powder and 4 mL isopropanol were ground in a ball mill for 4 h to obtain a homogeneous blend without any small clumps. ZIF-67 suspension of 1 mL was diluted with isopropanol to 10 mL and sonicated for 15 min. For the deposition of ZIF-67 thin film, the as-prepared ZIF-67 suspension was poured into a specially designed vessel. Then, two FTO ( $10 \text{ }\Omega\cdot\text{sq}^{-1}$ , Nippon Sheet Glass Co., Ltd., Japan) coated glass substrates were immersed vertically into the vessel, with one serving as an anode and another as a cathode. The distance between two electrodes was fixed at 1 cm. In the EPD process, various constant electric fields ranging from 20 to  $60 \text{ V}\cdot\text{cm}^{-1}$  were applied using a DC power supply. When a stable electric field is applied, the positively charged ZIF-67 nanoparticles begin to travel toward the cathode. After 1 min deposition, the FTO based cathode was taken out and dried naturally.

**2.2. Vulcanization of ZIF-67 Thin Films.** A combustion boat containing the as-prepared ZIF-67 thin film and 400 mg S powders was placed in a tube furnace. Then, the furnace was heated to a target temperature at a rate of  $5 \text{ }^\circ\text{C}\cdot\text{min}^{-1}$  and maintained at the target temperatures for 2 h in  $\text{N}_2$  atmosphere. After the furnace was completely cooled to room temperature, the combustion boat was

taken out and the film color was changed from purple to grayish black. The thin films vulcanized at 400, 450, 500, 550, and  $575 \text{ }^\circ\text{C}$  were named as S-400, S-450, S-500, S-550, and S-575, respectively.

**2.3. Characterization of Materials.** The morphologies of the thin films were observed using a scanning electron microscope (SEM, FEI Nova Nano SEM 230). The elemental compositions were analyzed by energy dispersive spectroscopy (EDS) attached to the SEM. The crystalline structure of the samples was characterized by an X-ray powder diffractometer (XRD, RigakuD/max-2500,  $\text{Cu K}\alpha$ ). The microstructures of samples were determined by high resolution transmission electron microscopy (HRTEM, Tecnai G<sup>2</sup> F20). The chemical composition and the valence states of the samples were analyzed on an X-ray photoelectron spectrometer (XPS, AXIS ULTRA Al  $\text{K}\alpha$ ). Fourier transform infrared spectra (FTIR) were measured on a FTIR spectrophotometer (Nicolet 360) using KBr as pellets. The absorption spectra of ZIF-67 thin films were measured using a spectrophotometer (UV-2600, SHIMADZU) at room temperature.

**2.4. Electrochemical Measurements.** All electrochemical measurements were performed on a potentiostat (Solartron 1287/1260) with the prepared thin film electrode or bare glassy carbon electrode (GCE, diameter 3 mm) as the working electrode, Pt wire as the counter electrode, and saturated calomel electrode (SCE) as the reference electrode. Cyclic voltammetry (CV) was performed in 30 mM vanillin electrolyte with 0.05 M phosphate buffer solution (PBS) ( $\text{pH} = 7.0$ ) at a scan rate of  $50 \text{ mV}\cdot\text{s}^{-1}$ . Before measurement, the electrolyte was purged with Ar for 20 min to remove oxygen. The area of the working electrode was  $0.7 \text{ cm}^2$ . Electrochemical impedance spectroscopy (EIS) and Tafel polarization curves were measured on the symmetrical cells fabricated by two identical electrodes. The frequency range of EIS is from  $10^5$  to  $10^{-1}$  Hz. The scan rate for Tafel measurements is  $10 \text{ mV}\cdot\text{s}^{-1}$ .

## 3. RESULTS AND DISCUSSION

### 3.1. Characterization of the Deposited ZIF-67 Thin Films.

As shown in Figure 1a, the synthesized ZIF-67 particles

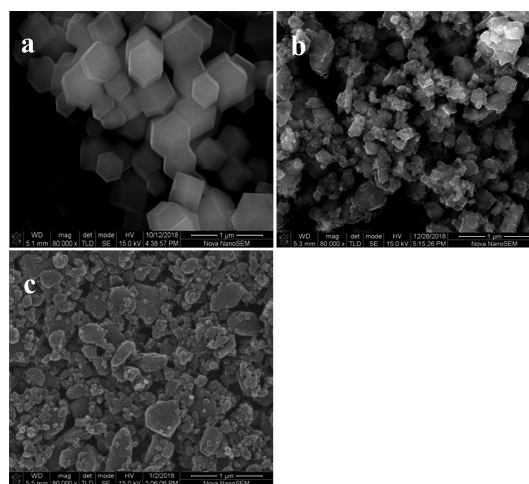


**Figure 1.** SEM images of as-prepared powders (a), as-ground powders (b), and EPD thin film (c) of ZIF-67.

exhibit a rhombic dodecahedron metal framework structure. SEM image of the ZIF-67 powder after being ground in the ball mill was shown in Figure 1b, and the morphology of the thin film formed by electrophoresis of ZIF-67 particles at an applied electric field of  $20 \text{ V}\cdot\text{cm}^{-1}$  was shown in Figure 1c. It was found that the particles after being ground and on the deposited thin film did not retain the complete rhombic dodecahedron structure of the original ZIF-67 particles. After being ground in the ball mill, the surface of the particles is

worn and defective. More cobalt ions are exposed on the surface due to the lack of ligand links, resulting in a partial positive charge on the surface of the ZIF-67 particle, which is very beneficial for electrophoresis. During the EPD process, the particles with the positive electrical charge were driven toward the negatively charged electrode. Furthermore, XRD patterns of the thin films (Figure 2) were measured to verify

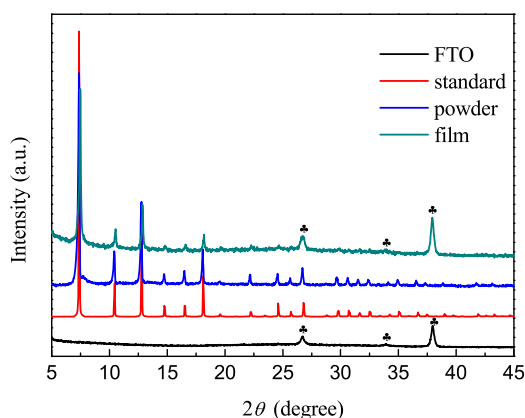


**Figure 2.** XRD patterns of ZIF-67 thin film, the standard ZIF-67, and powders.

the crystalline structural integrity of ZIF-67 deposited on the FTO electrode. The crystalline structure of the deposited thin films is similar to that of the powders, which demonstrates that the crystalline structure is not damaged during the EPD process. In order to better understand the effect of applied electric field during electrophoresis on the thickness and surface coverage of the deposited films, a series of ZIF-67 thin films were prepared under different electric fields from 20 to 60  $\text{V}\cdot\text{cm}^{-1}$ . The corresponding SEM cross section images of different ZIF-67 thin films were shown in Figure 3. It is clear that the film thickness can be controlled by the applied electric field as the deposition time is fixed as 1 min. Upon changing the electric field from 20 to 60  $\text{V}\cdot\text{cm}^{-1}$ , the film thickness could increase from 1.2 to 7.0  $\mu\text{m}$ . In addition, the continuous and dense ZIF-67 thin films could be obtained on the FTO substrate under different applied electric fields, when the films were deposited within 1 min (Figure 1S). Figure 4 shows UV-vis absorption spectra of ZIF-67 thin films grown at different electric fields of EPD and ZIF-67 powder in solution. The absorption peak position of different thin films is almost same, and it is also same as that of ZIF-67 powder in solution. It can be obviously seen that the absorption value of the ZIF-67 thin films increases as the deposition electric field was increased. However, the absorbance is not linearly increased with the film thickness (Figure 2S), indicating that the density of the deposited thin film is increased with the film thickness.

**3.2. Characterization of the Vulcanized ZIF-67 Thin Films.** Due to the flexibility of electrophoretic depositions, other MOF materials can also be deposited by this method to form the thin film electrode. In addition, the prepared thin film can be calcined to form some new film electrode materials, which have been applied in various aspects.<sup>28</sup> Here, the deposited ZIF-67 thin films were vulcanized with S powders to further form porous  $\text{Co}_9\text{S}_8$  thin films. The XRD patterns of the ZIF-67 thin films vulcanized at different temperatures were shown in Figure 5. The diffraction peaks marked with rhombus are indexed to  $\text{Co}_9\text{S}_8$  phase (JCPDS No. 02-1459) except one

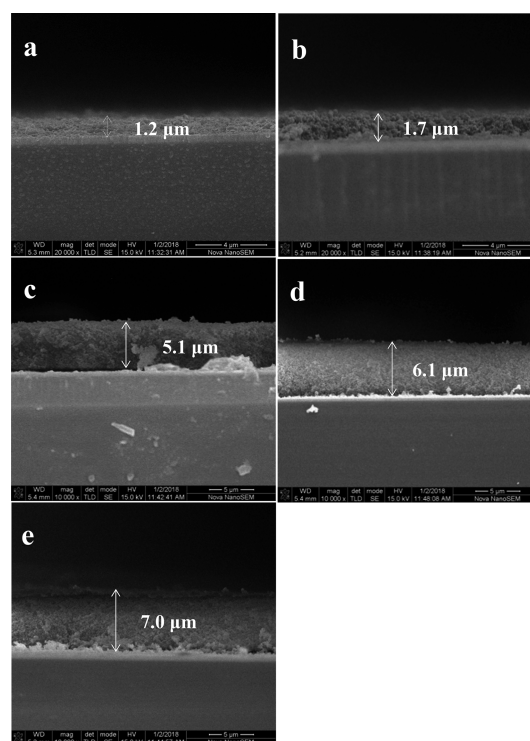


**Figure 3.** SEM cross sectional images of the thin films deposited under different electric fields of EPD: (a) 20, (b) 30, (c) 40, (d) 50, and (e) 60  $\text{V}\cdot\text{cm}^{-1}$ .

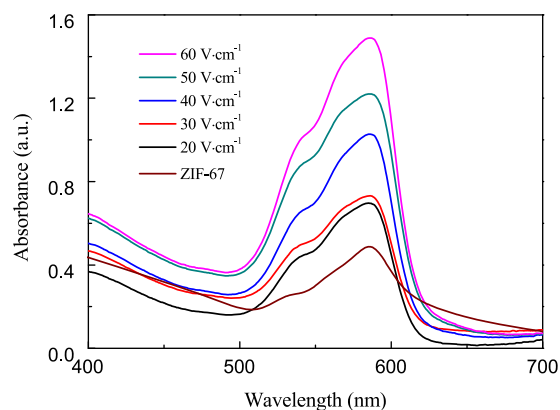


**Figure 4.** UV-vis absorption spectra of ZIF-67 thin films deposited under different electric fields and ZIF-67 in solution.

peak marked with heart belonging to  $\text{Co}_2\text{C}$  phase (JCPDS No. 65-1457). Obviously, ZIF-67 is not fully converted into single  $\text{Co}_9\text{S}_8$  phase. The complicated phases mainly consist of  $\text{Co}_9\text{S}_8$  phase with a small amount of  $\text{Co}_2\text{C}$  phase. However, almost all the peaks corresponding to ZIF-67 disappear indicating the rapid conversion from ZIF-67 thin film to  $\text{Co}_9\text{S}_8$  thin film by the vulcanization process. Using the Scherrer equation, the average crystal size of the  $\text{Co}_9\text{S}_8$  nanoparticles formed at 500  $^\circ\text{C}$  is estimated to be about 53 nm based on the full width at half-maximum ( $0.153^\circ$ ) of the (311) peak.

SEM images of the thin films vulcanized at different temperatures were shown in Figure 6. It is obvious that the morphologies of the  $\text{Co}_9\text{S}_8$  thin film depend on the vulcanization temperature. After the controlled reaction with S powders under  $\text{N}_2$ , the carbon skeleton shrinks sharply with the loss of other elements in ZIF structure, and some cracks

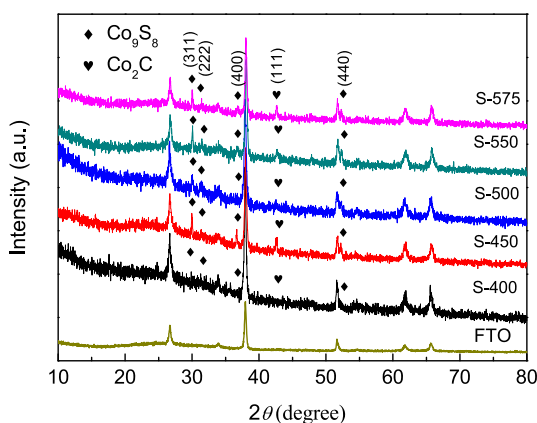


**Figure 5.** XRD patterns of the  $\text{Co}_9\text{S}_8$  thin films vulcanized at different temperatures and FTO.

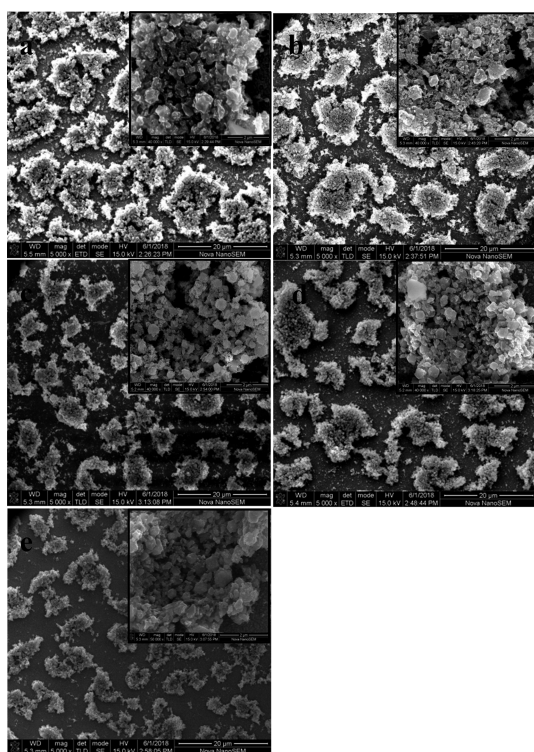


**Figure 6.** SEM images (low and high magnification) of the thin films of S-400 (a), S-450 (b), S-500 (c), S-550 (d), and S-575 (e).

appear between adjacent  $\text{Co}_9\text{S}_8$  structures. At 400 and 450 °C, the ZIF-67 thin films are not still completely corroded by the sulfur, maintaining the edges and corners of the carbon skeletons. However, after the vulcanization at 500 °C, the particles became round. It is worth noting that the film shows more porous structure composed of many nanoparticles, which facilitates easy penetration of the electrolyte into the thin film. However, at 550 and 575 °C, the high temperature vulcanization leads to the fusion and aggregation of the crystals to some extent, and the pores among the nanoparticles are significantly reduced and agglomeration occurs. In addition, the existence of Co, S, and C was confirmed in the composite thin film as shown in Figure S3. The cross-sectional images and corresponding element mapping of the S-500 thin film (Figure S4) further demonstrate the uniform distribution of the Co and S elements throughout the cross section, which

indicates that the vulcanization reaction has occurred inside the film. The  $\text{N}_2$  adsorption isotherm of S-500 thin film at 77 K showed a Brunauer–Emmett–Teller (BET) surface area of  $102.1 \text{ m}^2\cdot\text{g}^{-1}$  (Figure S5), which can provide a large interface to fully contact the electrolyte to promote the electrode reaction. The pore size distribution calculated using the Barrett–Joyner–Halenda (BJH) method showed the mesoporosity of the material with a relatively wide pore-size distribution in the range of 2–20 nm (inset in Figure S5).

In HRTEM image of the S-500 sample (Figure 7), it can be clearly seen that the nanoparticles are highly crystalline with

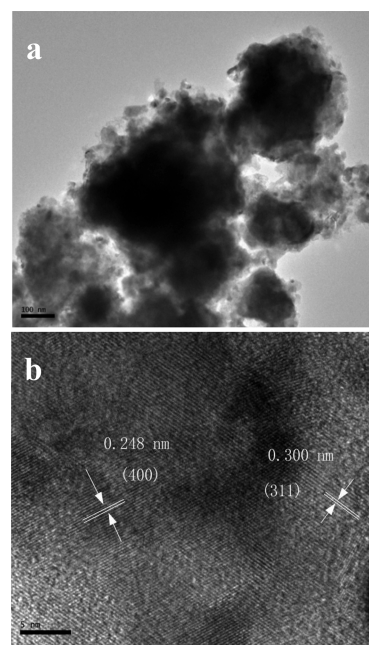


**Figure 7.** HRTEM of particles scraped from the S-500 thin film.

two sets of continuous lattice fringes with the  $d$ -spacing of 0.300 and 0.248 nm, which are correlated with the (311) and (400) crystal planes of  $\text{Co}_9\text{S}_8$  phase, respectively.

The thin films of S-500 and ZIF-67 were further characterized using FT-IR spectroscopy (Figure 8). ZIF-67 exhibits two intense bands at 1582 and  $1309 \text{ cm}^{-1}$ , which could be attributed to the C=N aromatic stretching and C–H vibration. The peak at  $426 \text{ cm}^{-1}$  is attributed to the Co–N

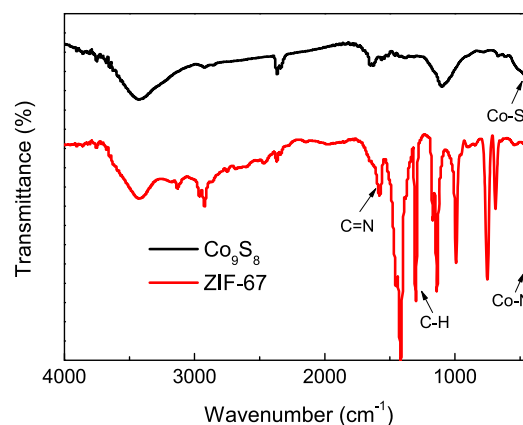


**Figure 8.** FTIR spectra of the thin film of S-500 and ZIF-67.

stretching. After the vulcanization process at 500 °C, the strong peak at 452  $\text{cm}^{-1}$  is contributed to the Co–S stretching. The sulfur atom coordinates with the cobalt atom to form the Co–S bond, accompanied by the breaking of the Co–N bond, and as a result, ZIF-67 is transformed into  $\text{Co}_9\text{S}_8$ .<sup>29,30</sup>

To determine the chemical states on the S-500 thin film, XPS spectra were measured and shown in Figure 9. It clearly suggests the presence of Co, C, S, N, O, and Sn in the as-obtained sample. Sn and O are from FTO, and C and N from the residual ZIF-67 skeleton. The high resolution XPS spectrum of Co 2p was shown in Figure 9b, where the peaks at 778.7, 781.7, and 786.6 eV can be specified as Co 2p<sub>3/2</sub>. The

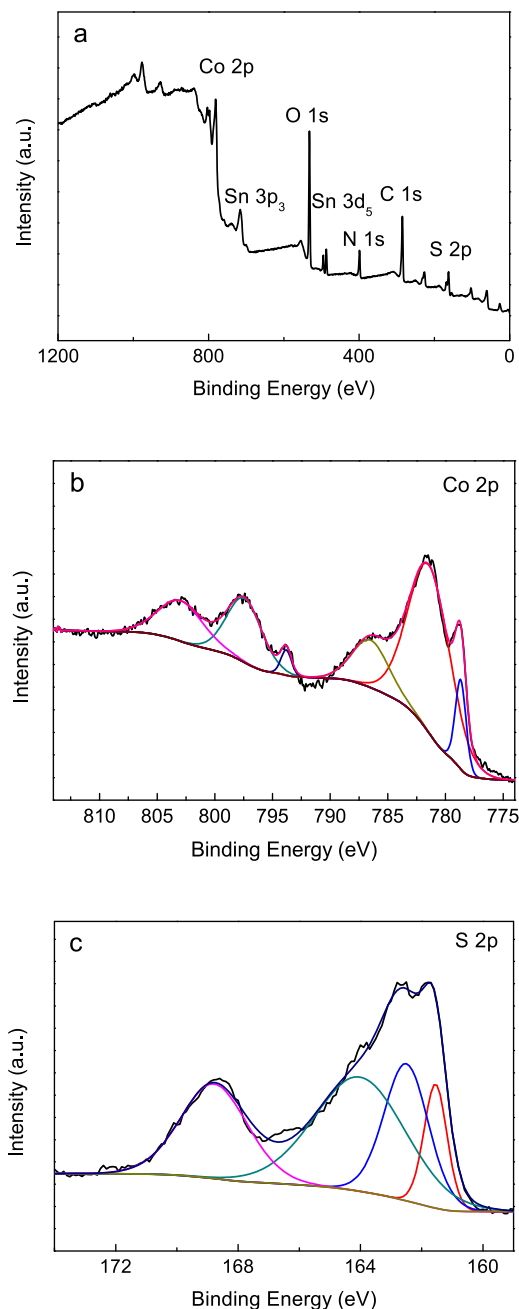
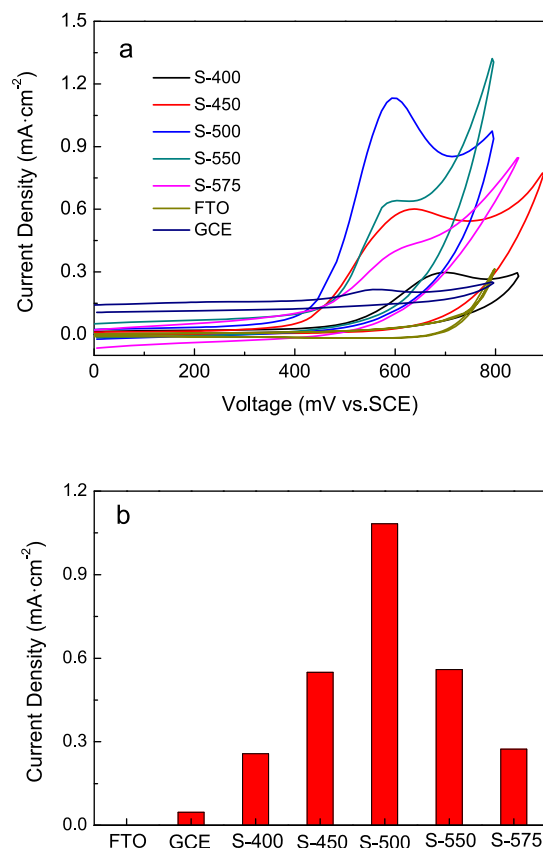


Fig. 9

**Figure 9.** XPS spectra of the S-500 thin film: (a) survey spectrum, (b) Co 2p, (c) S 2p.

fitting of Co 2p<sub>1/2</sub> peak shows three peaks with binding energies centered at 793.8, 797.6, and 803.2 eV, respectively. The peaks at 786.6 and 803.2 eV are the satellite peaks of 2p<sub>3/2</sub> and 2p<sub>1/2</sub>, respectively. The doublets appearing at 778.7 and 793.8 eV can be assigned to Co<sup>3+</sup> 2p<sub>3/2</sub> and 2p<sub>1/2</sub> states, while the doublets appearing at 781.7 and 797.6 eV belong to Co<sup>2+</sup> 2p<sub>3/2</sub> and 2p<sub>1/2</sub>. In the S 2p XPS spectrum (Figure 9c), the curve was fitted to show four peaks. They can be attributed to S in  $\text{Co}_9\text{S}_8$  (161.5 and 162.5 eV), C–S–C (163.8 eV), and  $\text{SO}_4^{2-}$  (168.6 eV), which is in good agreement with the previous report.<sup>31</sup> The presence of  $\text{SO}_4^{2-}$  may be related to partial oxidation of sulfur species by air on the surface of material.<sup>31</sup>

**3.3. Electrocatalytic Performance of the  $\text{Co}_9\text{S}_8$  Thin Films.** Based on the above discussions, the porous  $\text{Co}_9\text{S}_8$  thin film on FTO can be prepared from the ZIF-67 thin film. To explore potential applications of the porous  $\text{Co}_9\text{S}_8$  thin film, we used the  $\text{Co}_9\text{S}_8$  thin film electrodes to catalyze the oxidation of vanillin. The electrocatalytic activity of the  $\text{Co}_9\text{S}_8$  thin films were determined by cyclic voltammetry (CV) tests. And CV curves of the  $\text{Co}_9\text{S}_8$  thin film electrodes and bare GCE (Figure 10a) were recorded, respectively. There is an apparent



**Figure 10.** CV curves (a) and oxidation peak current density (b) of the thin films vulcanized at different temperatures and bare GCE.

oxidation peak of vanillin at 0.56 V vs SCE on bare GCE. In addition, for the  $\text{Co}_9\text{S}_8$  thin film electrodes prepared by vulcanization at different temperatures, the apparent oxidation peak of vanillin is located at around 0.60 V. In Figure 10b, it is clearly shown that the thin film electrode of S-500 has the largest peak current density compared to other electrodes. These results indicate that the thin film electrode of S-500

show better catalytic activity to oxidize vanillin than the bare GCE and others.<sup>30,32</sup>

The Tafel polarization curves of these samples were shown in Figure 11a, and the corresponding key parameters were

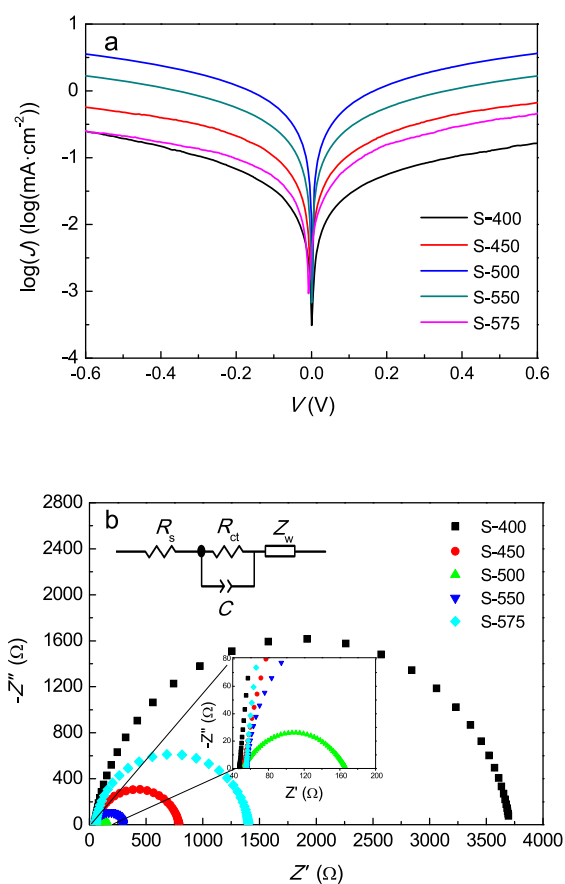


**Figure 11.** Tafel curves (a) and EIS (b) of the thin films vulcanized at different temperatures obtained by using symmetrical cells with two identical electrodes in 30 mM vanillin electrolyte.

**Table 1. Parameters Derived from Nyquist Plots of EIS and Tafel Polarization Curves**

electrode	$R_{ct}$ ( $\Omega$ )	$J_0$ ( $\text{mA}\cdot\text{cm}^{-2}$ )
S-400	3659.0	0.0466
S-450	739.4	0.1824
S-500	116.5	0.8586
S-550	241.1	0.4421
S-575	1347.0	0.0910

elaborated in Table 1. The exchange current density ( $J_0$ ) is the extrapolated intercepts of the anodic and cathodic branches of the corresponding Tafel curves and the higher values of  $J_0$  indicate the better catalytic activity.<sup>33</sup> As can be seen from Table 1, the thin film electrode of S-500 showed the highest  $J_0$  among all samples, and the tendency of the  $J_0$  totally agrees with the tendency of the peak current density observed in Figure 10b.

The interfacial properties of the electrode and the electrolyte affect the catalytic activity of the electrode toward vanillin. In order to further investigate the charge transfer process on the interface between the electrolyte of vanillin and the  $\text{Co}_9\text{S}_8$  thin

film electrode, EIS were performed by preparing typical sandwich structure of  $\text{Co}_9\text{S}_8$  electrode/electrolyte/ $\text{Co}_9\text{S}_8$  electrode. The EIS of the  $\text{Co}_9\text{S}_8$  thin film electrodes and the related equivalent circuit diagram were shown in Figure 11b. The interface properties can be evaluated by the resistance of the interface transfer electron ( $R_{ct}$ ). By fitting the EIS with the equivalent circuit,  $R_{ct}$  values were obtained and summarized in Table 1. The  $R_{ct}$  values of the  $\text{Co}_9\text{S}_8$  electrodes were in order of S-500 < S-550 < S-450 < S-575 < S-400. The smaller semicircle of the  $\text{Co}_9\text{S}_8$  electrodes obtained at different temperatures corresponds to the smaller  $R_{ct}$ , and the lower  $R_{ct}$  value of the electrodes indicates that the oxidation reaction at the electrode/electrolyte interface is faster. The results showed that S-500 has better electrocatalytic activity for vanillin than other electrodes. According to the various characterization measurements on the samples, we thought the best electrocatalytic activity of S-500 is attributed to its porous structure can be mostly survived and organic ligands of ZIF-67 can be almost removed after vulcanization under the optimized vulcanization temperature of 500 °C.

#### 4. CONCLUSIONS

In summary, uniform ZIF-67 thin films were prepared on FTO substrate by the electrophoretic deposition method. The film thickness can be adjusted by adjusting the applied electric field as the deposition time was fixed at 1 min. The deposited ZIF-67 thin films were further vulcanized to form the  $\text{Co}_9\text{S}_8$  thin films. The vulcanization temperature can affect the composition and porous structure. The  $\text{Co}_9\text{S}_8$  thin film show a satisfied catalytic activity to degrade vanillin, and the thin film electrode prepared by vulcanization at 550 °C has the best catalytic performance. It provides a viable method for the electrocatalytic detection of vanillin. The electrophoretic deposition method is very promising in the film formation of MOF materials and has better industrial application prospects.

#### ■ ASSOCIATED CONTENT

##### Supporting Information

The Supporting Information is available free of charge on the ACS Publications website at DOI: 10.1021/acs.inorgchem.8b03281.

SEM morphologies of ZIF-67 thin films deposited under different electric fields, relationship of the absorbance and the thickness of ZIF-67 thin films, the element mapping images, and  $\text{N}_2$  sorption isotherms of the S-500 thin film (PDF)

#### ■ AUTHOR INFORMATION

##### Corresponding Author

\*Email: hxyzyjb@mail.tjnu.edu.cn (J.Z.).

##### ORCID

Jingbo Zhang: 0000-0002-6672-2650

##### Notes

The authors declare no competing financial interest.

#### ■ ACKNOWLEDGMENTS

This work was financially supported by the National Nature Science Foundation of China (Grant No. 21273160), the Nature Science Foundation of Tianjin (Grant No. 14JCYBJC18000), and the Program for Innovative Research Team in University of Tianjin (TD13-S074).

## REFERENCES

- (1) Furukawa, H.; Ko, N.; Go, Y. B.; Aratani, N.; Choi, S. B.; Choi, E.; Yazaydin, A. O.; Snurr, R. Q.; O'Keeffe, M.; Kim, J.; Yaghi, O. M. Ultrahigh Porosity in Metal-Organic Frameworks. *Science* **2010**, *329*, 424–428.
- (2) Li, J. R.; Sculley, J.; Zhou, H. C. Metal-Organic Frameworks for Separations. *Chem. Rev.* **2012**, *112*, 869–932.
- (3) Ma, L. Q.; Abney, C.; Lin, W. B. Enantioselective Catalysis with Homochiral Metal-Organic Frameworks. *Chem. Soc. Rev.* **2009**, *38*, 1248–1256.
- (4) Kreno, L. E.; Leong, K.; Farha, O. K.; Allendorf, M.; Van Duyne, R. P.; Hupp, J. T. Metal-Organic Framework Materials as Chemical Sensors. *Chem. Rev.* **2012**, *112*, 1105–1125.
- (5) Taylor, J. M.; Dawson, K. W.; Shimizu, G. K. A Water-Stable Metal-Organic Framework with Highly Acidic Pores for Proton-Conducting Applications. *J. Am. Chem. Soc.* **2013**, *135*, 1193–1196.
- (6) Mao, J.; Yang, L.; Yu, P.; Wei, X. W.; Mao, L. Q. Electrocatalytic four-electron reduction of oxygen with Copper (II)-based Metal-Organic Frameworks. *Electrochem. Commun.* **2012**, *19*, 29–31.
- (7) Hu, H.; Han, L.; Yu, M. Z.; Wang, Z. Y.; Lou, X. W. Metal-Organic-Framework-Engaged Formation of Co Nanoparticle-Embedded carbon@Co<sub>9</sub>S<sub>8</sub> double-shelled nanocages for efficient oxygen reduction. *Energy Environ. Sci.* **2016**, *9*, 107–111.
- (8) Gao, Y. X.; Yu, G.; Liu, K.; Wang, B. Luminescent Mixed-Crystal Ln-MOF Thin Film for the Recognition and Detection of Pharmaceuticals. *Sens. Actuators, B* **2018**, *257*, 931–935.
- (9) Ferey, G.; Millange, F.; Morcrette, M.; Serre, C.; Doublet, M. L.; Greneche, J. M.; Tarascon, J. M. Mixed-valence Li/Fe-based Metal-Organic Frameworks with both Reversible Redox and Sorption Properties. *Angew. Chem., Int. Ed.* **2007**, *46*, 3259–3263.
- (10) Diaz, R.; Orcajo, M. G.; Botas, J. A.; Calleja, G.; Palma, J. Co8-MOF-5 as Electrode for Supercapacitors. *Mater. Lett.* **2012**, *68*, 126–128.
- (11) Shekhah, O.; Liu, J.; Fischer, R. A.; Woll, Ch. MOF thin films: Existing and Future Applications. *Chem. Soc. Rev.* **2011**, *40*, 1081–1106.
- (12) Hermes, S.; Schroder, F.; Chelmoski, R.; Wöll, C.; Fischer, R. A. Selective Nucleation and Growth of Metal-Organic Open Framework Thin Films on Patterned COOH/CF<sub>3</sub>-Terminated Self-Assembled Monolayers on Au(111). *J. Am. Chem. Soc.* **2005**, *127*, 13744–13745.
- (13) Shekhah, O.; Wang, H.; Kowarik, S.; Schreiber, F.; Paulus, M.; Tolan, M.; Sternemann, C.; Evers, F.; Zacher, D.; Fischer, R. A.; Wöll, C. Step-by-Step Route for the Synthesis of Metal-Organic Frameworks. *J. Am. Chem. Soc.* **2007**, *129*, 15118–15119.
- (14) Yoo, Y.; Jeong, H. K. Rapid fabrication of Metal Organic Framework Thin Films using Microwave-Induced Thermal Deposition. *Chem. Commun.* **2008**, *0*, 2441–2443.
- (15) Wu, Y.; Li, F.; Liu, H.; Zhu, W.; Teng, M.; Jiang, Y.; Li, W.; Xu, D.; He, D.; Hannam, P.; Li, G. Electrospun Fibrous Mats as Skeletons to Produce Free-Standing MOF Membranes. *J. Mater. Chem.* **2012**, *22*, 16971–16978.
- (16) Chen, Y.; Li, S.; Pei, X.; Zhou, J.; Feng, X.; Zhang, S.; Cheng, Y.; Li, H.; Han, R.; Wang, B. A Solvent-Free Hot-Pressing Method for Preparing Metal-Organic-Framework Coatings. *Angew. Chem., Int. Ed.* **2016**, *55*, 3419–3423.
- (17) Vander Biest, O. O.; Vandeperre, L. J. Electrophoretic Deposition of Materials. *Annu. Rev. Mater. Sci.* **1999**, *29*, 327–352.
- (18) Veeramani, V.; Madhu, R.; Chen, S. M.; Veerakumar, P.; Syu, J. J.; Liu, S. B. Cajeput Tree Bark Derived Activated Carbon for the Practical Electrochemical Detection of Vanillin. *New J. Chem.* **2015**, *39*, 9109–9115.
- (19) Deng, P.; Xu, Z.; Zeng, R.; Ding, C. Electrochemical Behavior and Voltammetric Determination of Vanillin Based on an Acetylene Black Paste Electrode Modified with Graphene-Polyvinylpyrrolidone Composite Film. *Food Chem.* **2015**, *180*, 156–163.
- (20) Ni, Y.; Zhang, G.; Kokot, S. Simultaneous Spectrophotometric Determination of Maltol, Ethyl Maltol, Vanillin and Ethyl Vanillin in Foods by Multivariate Calibration and Artificial Neural Networks. *Food Chem.* **2005**, *89*, 465–473.
- (21) Ainscough, E. W.; Brodie, A. M. The Determination of Vanillin in Vanilla extract: An Analytical Chemistry Experiment. *J. Chem. Educ.* **1990**, *67*, 1070–1072.
- (22) López, R.; Aznar, M.; Cacho, J.; Ferreira, V. Determination of Minor and Trace Volatile Compounds in Wine by Solid-Phase Extraction and Gas Chromatography with Mass Spectrometric Detection. *J. Chromatogr. A* **2002**, *966*, 167–177.
- (23) Peng, H.; Wang, S.; Zhang, Z.; Xiong, H.; Li, J.; Chen, L.; Li, Y. Molecularly Imprinted Photonic Hydrogels as Colorimetric Sensors for Rapid and Label-free Detection of Vanillin. *J. Agric. Food Chem.* **2012**, *60*, 1921–1928.
- (24) Bettazzi, F.; Palchetti, I.; Sisalli, S.; Mascini, M. A Disposable Electrochemical Sensor for Vanillin Detection. *Anal. Chim. Acta* **2006**, *555*, 134–138.
- (25) Feng, F.; Yang, X.; Gao, S. Y.; Shi, J. L.; Cao, R. Facile and Rapid Growth of Nanostructured Ln-BTC Metal-Organic Framework Films by Electrophoretic Deposition for Explosives Sensing in Gas and Cr<sup>3+</sup> Detection in Solution. *Langmuir* **2017**, *33*, 14238–14243.
- (26) Hod, I.; Bury, W.; Karlin, D. M.; Deria, P.; Kung, C. W.; Katz, M. J.; So, M.; Klahr, B.; Jin, D.; Chung, N. Y. W.; Odom, T. W.; Farha, O. K.; Hupp, J. T. Directed Growth of Electroactive Metal-Organic Framework Thin Films Using Electrophoretic Deposition. *Adv. Mater.* **2014**, *26*, 6295–6300.
- (27) Jiang, Z.; Li, Z. P.; Qin, Z. H.; Sun, H. Y.; Jiao, X. L.; Chen, D. R. LDH Nanocages Synthesized with MOF Templates and Their High Performance as Supercapacitors. *Nanoscale* **2013**, *5*, 11770–11775.
- (28) Xu, W. J.; Sun, Y. X.; Ding, B.; Zhang, J. B. Zeolitic-Imidazolate Frameworks Derived Pt-free Counter Electrodes for High-Performance Quantum Dot-Sensitized Solar Cells. *R. Soc. Open Sci.* **2018**, *5*, 180335.
- (29) Jin, M.; Lu, S. Y.; Ma, L.; Gan, M. Y.; Lei, Y.; Zhang, X. L.; Fu, G.; Yang, P. S.; Yan, M. F. Different Distribution of In-situ Thin Carbon Layer in Hollow Cobalt Sulfide Nanocages and Their Application for Supercapacitors. *J. Power Sources* **2017**, *341*, 294–301.
- (30) Sivakumar, M.; Sakthivel, M.; Chen, S. M. Simple Synthesis of Cobalt Sulfide Nanorods for Efficient Electrocatalytic Oxidation of Vanillin in Food Samples. *J. Colloid Interface Sci.* **2017**, *490*, 719–726.
- (31) Feng, L. L.; Fan, M. H.; Wu, Y. Y.; Liu, Y. P.; Li, G. D.; Chen, H.; Chen, W.; Wang, D. J.; Zou, X. X. Metallic Co<sub>9</sub>S<sub>8</sub> Nanosheets Grown on Carbon Cloth as Efficient Binder-Free Electrocatalysts for the Hydrogen Evolution Reaction in Neutral Media. *J. Mater. Chem. A* **2016**, *4*, 6860–6867.
- (32) Hardcastle, J. L.; Paterson, C. J.; Compton, R. G. Biphasic Sono-electroanalysis: Simultaneous Extraction From, and Determination of Vanillin in Food Flavoring. *Electroanalysis* **2001**, *13*, 899–905.
- (33) Niu, Y. D.; Qian, X.; Zhang, J.; Wu, W. M.; Liu, H. Y.; Xu, C.; Hou, L. X. Stepwise Synthesis of CoS<sub>2</sub>-C@CoS<sub>2</sub> Yolk-shell Nanocages with much Enhanced Electrocatalytic Performances both in Solar Cells and Hydrogen Evolution Reactions. *J. Mater. Chem. A* **2018**, *6*, 12056–12065.